

Simulating terahertz field-induced transient ferroelectricity in quantum paraelectric SrTiO₃

Dongbin Shin,^{1,*} Simone Latini,¹ Christian Schäfer,¹ Shunsuke A. Sato,^{1,2}
Edoardo Baldini,³ Umberto De Giovannini,^{1,4} Hannes Hübener,¹ and Angel Rubio^{1,4,5,†}

¹*Max Planck Institute for the Structure and Dynamics of Matter and
Center for Free Electron Laser Science, 22761 Hamburg, Germany*

²*Center for Computational Sciences,
University of Tsukuba, Tsukuba 305-8577, Japan*

³*Department of Physics, Massachusetts Institute of Technology,
02139 Cambridge, Massachusetts, USA*

⁴*Nano-Bio Spectroscopy Group, Departamento de Física de Materiales,
Universidad del País Vasco UPV/EHU- 20018 San Sebastián, Spain*

⁵*Center for Computational Quantum Physics (CCQ),
The Flatiron Institute, 162 Fifth avenue, New York NY 10010.*

(Dated: June 9, 2021)

Abstract

Recent experiments have demonstrated that intense terahertz (THz) fields can induce a transition from the quantum paraelectric to the ferroelectric phase of SrTiO₃. Here, we investigate this THz field-induced transient ferroelectric phase transition by solving the time-dependent lattice Schrödinger equation based on first-principles calculations. We find that transient ferroelectricity originates from a light-induced mixing between ground and first excited lattice states in the quantum paraelectric phase. In agreement with the experimental findings, our study shows that the non-oscillatory second harmonic generation signal can be evidence of transient ferroelectricity in SrTiO₃. We reveal the microscopic details of this exotic phase transition and highlight that this phenomenon is a unique behavior of the quantum paraelectric phase.

Ultrafast light-induced dynamics provides attractive physical phenomena beyond the steady state of materials. Recent studies have shown that driving materials out of their original equilibrium state can induce complex phase transitions or largely modify properties and functionalities of materials [1–6]. Theoretical works have suggested that many of these THz field-induced phenomena are closely related with nonlinear phonon interactions [7–10]. For example, by applying a terahertz (THz) pulse, a high temperature (100 K) superconducting state has been experimentally observed in K₃C₆₀ which exhibits low critical temperature (30 K) at its ground state [1, 11, 12]. Possible topological phase transitions induced by THz pulses has also been demonstrated in layered materials such as 1T-WTe₂, ZrTe₅, and graphene [13–15]. Another paradigmatic manifestation of the THz-matter interaction is the transformation of paraelectric SrTiO₃ into ferroelectric phase [3, 4].

Unlike other transition metal perovskite materials as BaTiO₃ and PbTiO₃, at low temperature SrTiO₃ does not show a paraelectric-to-ferroelectric phase transition [16–26]. The origin of this phenomenon lies in the potential energy surface of SrTiO₃ along the ferroelectric soft (FES) mode, which has a shallow double-well potential at the low temperature [24–26]. Despite classically favoring a ferroelectric phase, SrTiO₃ remains in the high symmetry phase due to nuclear quantum fluctuations [25, 26]. The corresponding low-temperature phase of SrTiO₃ is therefore a quantum paraelectric phase. Recent first-principles calculations revealed that both quantum fluctuation and the nonlinear interaction between the FES mode and lattice strain are required to describe the quantum paraelectric phase in SrTiO₃ [26]. The inclusion of these effects enables to computationally reproduce temperature dependent

properties, such as the energy of the FES mode and the dielectric constant [24, 26]. Relying on such a first principles description, an optically stabilized ferroelectric ground state of SrTiO₃ in a cavity has been theoretically demonstrated [27].

Here, we investigate the THz field-induced non-equilibrium transient ferroelectricity of the quantum paraelectric state of SrTiO₃ based on a lattice model derived from extensive first principles calculations [26]. By solving the time-dependent lattice Schrödinger-Langevin equation, we show that a transient ferroelectric state can be obtained in SrTiO₃ by illumination with a single cycle THz pulse. We find that this transient ferroelectricity originates from the mixing between ground and first excited states of the lattice wavefunction. Based on time-dependent density functional theory (TDDFT) calculations, we obtain a non-oscillatory second harmonic generation (SHG) signal and find that it is a signature of the induced broken symmetry, in agreement with the conclusions drawn from experimental observations [3, 4]. Lastly, we discuss the conditions of THz pulse frequency and dissipation rate for the transient ferroelectricity.

By solving a time-dependent lattice Schrödinger-Langevin equation, we investigate the THz field-induced transient ferroelectric transition from quantum paraelectric SrTiO₃ as depicted in Fig. 1(a). Recent first principles-based study reported that the quantum paraelectric state in SrTiO₃ can be described by the two-dimensional (2D) lattice Schrödinger equation [26]. The 2D effective potential for quantum paraelectric SrTiO₃ consists of FES mode Q_f and the lattice expansion/contraction along the FES mode direction Q_c , as shown in Figs. 1(b) and 1(c). It is constructed from fitting the calculated total energy as a function of geometry distortions as follows: $\hat{V}_{2D}^{\text{FES},c} = \sum_{i=1}^{12} k_{f,i} \hat{Q}_f^{2i} + \sum_{j=2}^{10} k_{c,j} \hat{Q}_c^j + \sum_{i=1}^{12} \sum_{j=1}^{10} k_{fc,i,j} \hat{Q}_f^{2i} \hat{Q}_c^j$ [26, 28]. For the DFT total energy calculation, we used the QUANTUM ESPRESSO package with the projector augmented wave method and a plane-wave basis set with 70 Ry energy cut-off [29]. The electron-electron exchange and correlation potentials are described through the Perdew-Berke-Ernzerhof functional [30]. We considered the $\sqrt{2} \times \sqrt{2} \times 2$ tetragonal unit cell for the low temperature phase of SrTiO₃ and we sampled the Brillouin zone with a $6 \times 6 \times 4$ \mathbf{k} -point grid. Details on the parameters used the 2D effective potential energy surface are summarized in the Supplemental Material [28]. To describe the effect of the THz pump pulse on quantum paraelectric SrTiO₃, we solved the time-dependent 2D lattice Schrödinger-Langevin equation $i\hbar \frac{d}{dt} \psi = \hat{H}_{2D} \psi + \gamma(\hat{S} - \langle \hat{S} \rangle) \psi$, with the Hamiltonian $\hat{H}_{2D}[Q_f, Q_c, t] = \hat{P}_f^2/2M_f + \hat{P}_c^2/2M_c + \hat{V}_{2D}^{\text{FES},c} + E_{ext}(t)Z_f \hat{Q}_f$. The

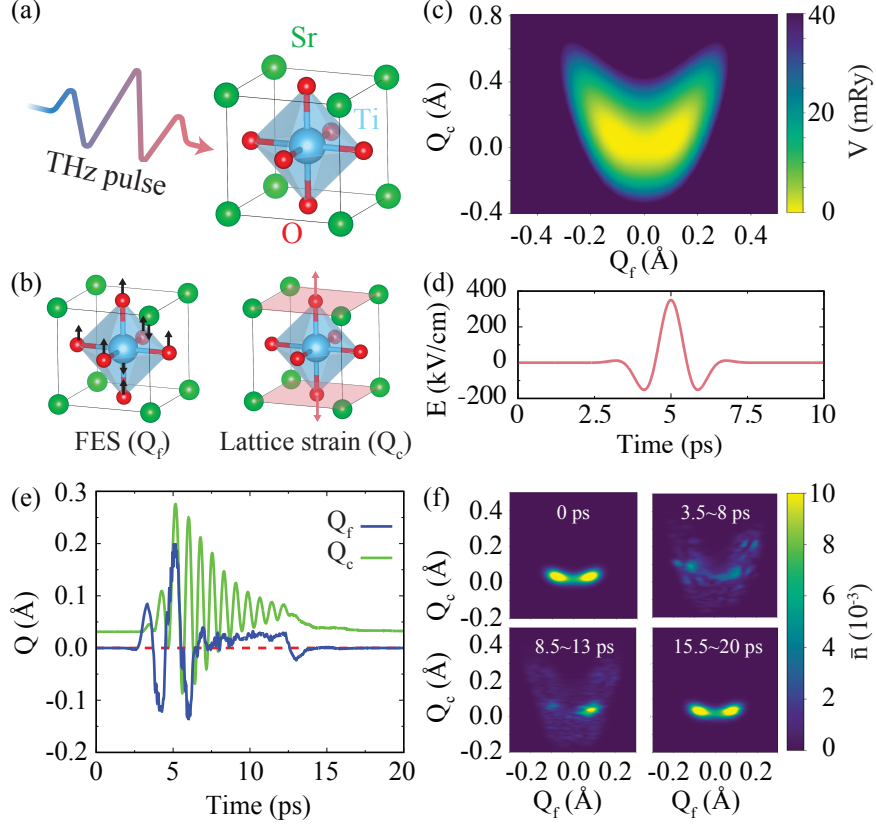


FIG. 1. THz field-induced transient ferroelectricity in SrTiO₃. (a) Schematic image of the THz pulse applied to SrTiO₃. (b) Schematic image of the atomic displacements involved in the FES mode (Q_f) and lattice strain (Q_c). (c) Two-dimensional potential energy surface of SrTiO₃ along the FES mode (Q_f) and lattice (Q_c) coordinates. (d) Time profile of single-cycle THz pulse with 0.5 THz frequency. (e) Time profiles of the expectation value of the FES mode (Q_f) and lattice (Q_c) perturbed by the THz pulse. Red dashed line in (e) is a guide to the eye for the zero value. (f) Variation of the time-averaged lattice density perturbed by the THz pulse.

effective mass of the FES mode is $M_f = 1.76 \times 10^{-25}$ kg. The mass of the tetragonal cell is used as the lattice effective mass ($M_c = \sum_i M_i = 1.22 \times 10^{-24}$ kg). The γ and $\hat{S}[Q_f, Q_c, t] = \arg[\psi(Q_f, Q_c, t)]$ are the dissipation rate and the phase of the wavefunction respectively [31, 32]. We used a dissipation rate of $\gamma = 0.9$ THz for the FES mode as reported by recent spectroscopic measurements [33]. We considered the interaction between the FES mode and the THz pulse ($H_{int} = E_{ext}(t)Z_f\hat{Q}_f$) to be linear in the external field strength and the electric dipole generated by Q_f with its Born effective charge ($Z_f = 36e$) calculated under the dipole approximation. Details on the time-dependent Schrödinger-Langevin equation are discussed in the Supplemental Material [28].

We simulated the action of a single-cycle THz pulse on the low temperature quantum

paraelectric state of SrTiO₃, choosing it to be resonant with the frequency of the FES mode (0.5 THz) and with a maximum strength of 375 kV/cm, as shown in Fig. 1(d). This THz pulse perturbs the quantum paraelectric ground state $\psi_0(Q_f, Q_c, t = 0)$ and induces a variation in the expectation values of $Q_f(t)$ and $Q_c(t)$, as shown in Fig. 1(e). It is notable that the asymmetric potential along Q_c provides non-zero value ($Q_c(t = 0) = 31 \text{ m\AA}$) in the ground state because of quantum fluctuations [26]. The time-profile of the FES mode exhibits a non-oscillatory component between 7.5 and 15 ps time period. Because the FES mode is directly related to the electric polarization of the system ($P = Z_f Q_f$), this plateau indicates that the single-cycle THz pulse induces a transient ferroelectric phase. We also found that the THz pulse transiently elongates the lattice (Q_c), providing a deeper double well for the FES mode, as shown in Fig. 1(c) [26]. To understand the variation of the 2D lattice state, we evaluated the time-averaged lattice densities ($\bar{n}(t_1, t_0) = \int_{t_0}^{t_1} |\psi(Q_f, Q_t, t)|^2 dt$) for a given period of time, as displayed in Fig. 1(f). In the ground state ($t = 0$ ps), the time-averaged lattice density is delocalized over the double well potential along the Q_f direction, indicating a quantum paraelectric ground state. At the time delay $t = 3.5 \sim 7$ ps, the applied THz pulse strongly perturbs the lattice density. Upon application of the THz pulse ($t = 7.5 \sim 14$ ps), the lattice density localizes in one of the two wells signaling the emergence of a transient ferroelectric state. Due to dissipation, the excited state finally returns to the quantum paraelectric phase ($t = 15 \sim 20$ ps).

This THz field-induced ferroelectric transition originates from the excitation between the ground and first excited states of the lattice wavefunction. As shown in Fig. 1(e) and upper panel of Fig. 2(a), the THz pulse with 375 kV/cm induces a transient ferroelectric state that is characterized by the non-oscillatory behavior of Q_f between 8 and 12.5 ps. On the other hand, transient ferroelectricity can be barely triggered by a THz pulse with higher strength (500 kV/cm). The THz-induced ferroelectricity and its strength dependence can be explained in terms of phonon excitation by the THz pulse, as displayed in Fig. 2(b). The THz pulse with appropriate strength allows excitation to the first excited state (ψ_1) from the ground state (ψ_0) shown in Figs. 2(c) and 2(d). It is worth noting that the linear combination between ground and first excited states provides two degenerate ferroelectric states, which have opposite electric polarization ($\psi_0 + \psi_1$ and $\psi_0 - \psi_1$). When a single-cycle THz pulse is applied, the symmetry of the excited state along Q_f is broken and ferroelectricity emerges. By contrast, a high field strength THz pulse promotes transitions to

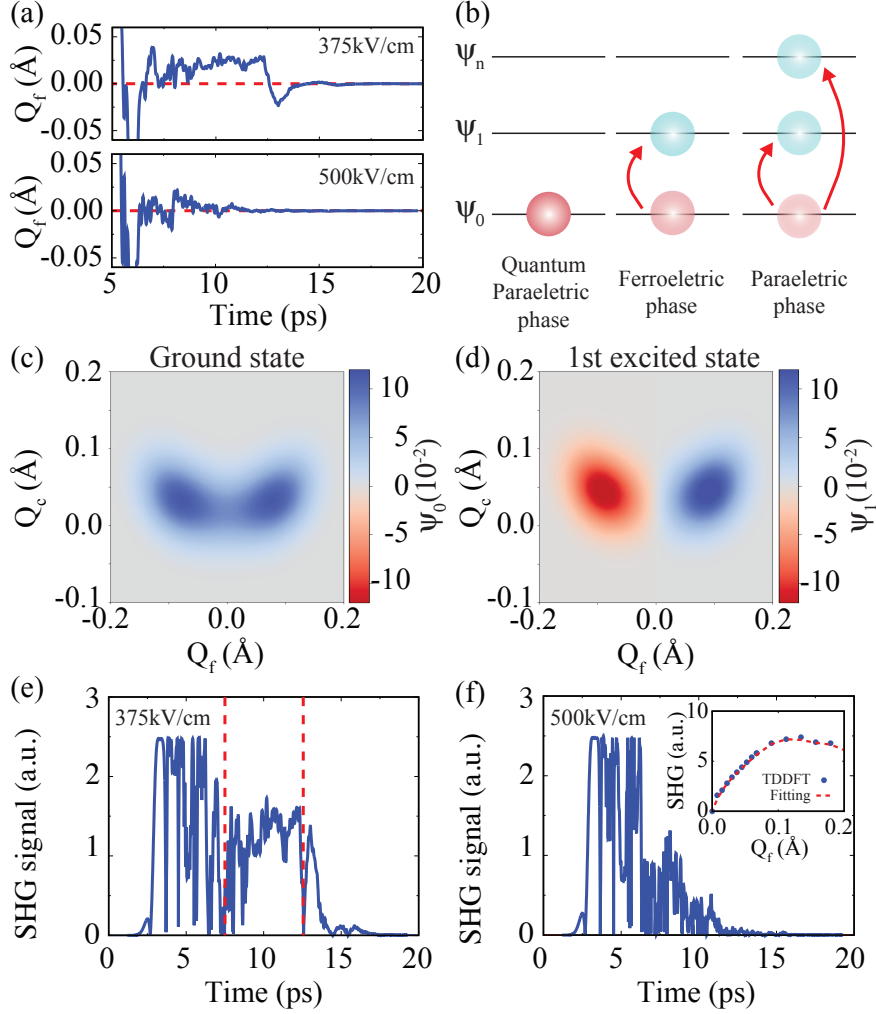


FIG. 2. Mechanism of the THz field-induced phase transition from the quantum paraelectric state. (a) Time profiles of expectation value of FES mode (Q_f) perturbed by a THz pulse with 375 kV/cm (top panel) and 500 kV/cm (bottom panel) field strength. (b) Schematic image of the phase transition from the quantum paraelectric state. (c) Ground and (d) first excited states of the quantum paraelectric phase in SrTiO₃. Time profile of the SHG signal induced by a THz pulse with (e) 375 kV/cm and (f) 500 kV/cm. The red dashed line in (a) is a guide to the eye for the zero level. The red dashed line in (E) is a guide to the eye for range of the transient ferroelectric state. The inset of (f) shows the relation between the SHG signal and the FES mode distortion evaluated by TDDFT calculations.

excited states much higher in energy and produces a light-mixed state equivalent to thermally excited paraelectric state, which spreads over the full double-well potential. Details about the ferroelectric lattice wavefunction in the quantum paraelectric phase are discussed in the Supplemental Material [28].

In recent experimental results [3, 4], the SHG signal of a delayed near-infrared probe has been interpreted as a signature of the light-induced ferroelectricity in SrTiO₃. To evaluate the

SHG signal from the lattice wavefunction, we calculated the relation between the SHG signal and Q_f from TDDFT calculation with distorted geometry along the FES mode direction (see the inset of Fig. 3(f)) [34]. With tetragonal SrTiO₃ geometries distorted along the FES mode direction, we evaluated the response of the current by applying a 1.55 eV probe pulse with 40 fs duration. To connect the time-profile of SHG to the 2D model quantities, the obtained SHG signal is fitted as a function of Q_f with polynomial parameters: $\text{SHG}(Q_f) = \sum_i^3 c_i |Q_f|^i$. Relying on this relation, we estimated the time-profile of the SHG signal, as shown in Figs. 2(e) and 2(f). The SHG signal induced by the 375 kV/cm THz pulse exhibits the non-oscillatory behavior similar to the time-profile of Q_f . On the other hand, excitation with THz pulse of higher intensity (500 kV/cm) leads to a fast decay of the SHG signal, resulting in oscillations that touch zero. Similar to the experimental observations [3, 4], our TDDFT calculation reveals that the non-oscillatory behavior of the SHG signal can be a key fingerprint of the transient ferroelectric state. Details on the procedure used to evaluate the SHG signal from TDDFT calculations are discussed in the Supplemental Material [28].

Terahertz field-induced transient ferroelectricity can be obtained with a single resonant THz pulse and realistic dissipation. To investigate the condition for the THz-induced transient ferroelectricity, we evaluated the time-averaged Q_f value as follows: $Q_f^{avg} = \frac{1}{t_1} \int_{t_0}^{t_0+t_1} Q_f(t) dt$, where t_0 is the time at the end point of the pulse and $t_1 = 12$ ps. First, we investigated the effect of the THz pulse frequency on transient ferroelectricity, as shown in Fig. 3(a). We employed a single-cycle THz pulse with frequency ω , $E(t) = E_0 \cos(2\pi\omega t) \sin^2(\frac{2\pi}{10}\omega t)$, as shown in Fig. 1(d). When we apply the resonant THz pulse ($\omega = 0.5$ THz) with the dissipation rate $\gamma = 0.9$ THz, we observe non-oscillatory behavior with large values of Q_f^{avg} for a wide range of THz field strength. On the other hand, a near-resonant THz pulse with $\omega = 0.8$ THz provides suppressed Q_f^{avg} values and an off-resonant THz pulse with $\omega = 1.0$ THz gives negligible Q_f^{avg} values. As a consequence, while a non-oscillatory behavior of $Q_f(t)$ is observed with resonant $\omega = 0.5$ THz and near-resonant $\omega = 0.8$ THz frequencies, there is no plateau with off-resonant frequency ($\omega = 1.0$ THz), as shown in Fig. 3(b). This result indicates that the resonant THz pulse effectively excites the FES mode from the ground state to the first excited state, and transient ferroelectricity is formed as a superposition of the ground and first excited states. In contrast, off-resonant THz pulses hardly lead to transient ferroelectricity. It is notable that single-cycle THz pulses, which contain a broad frequency spectrum, allow for the excitation

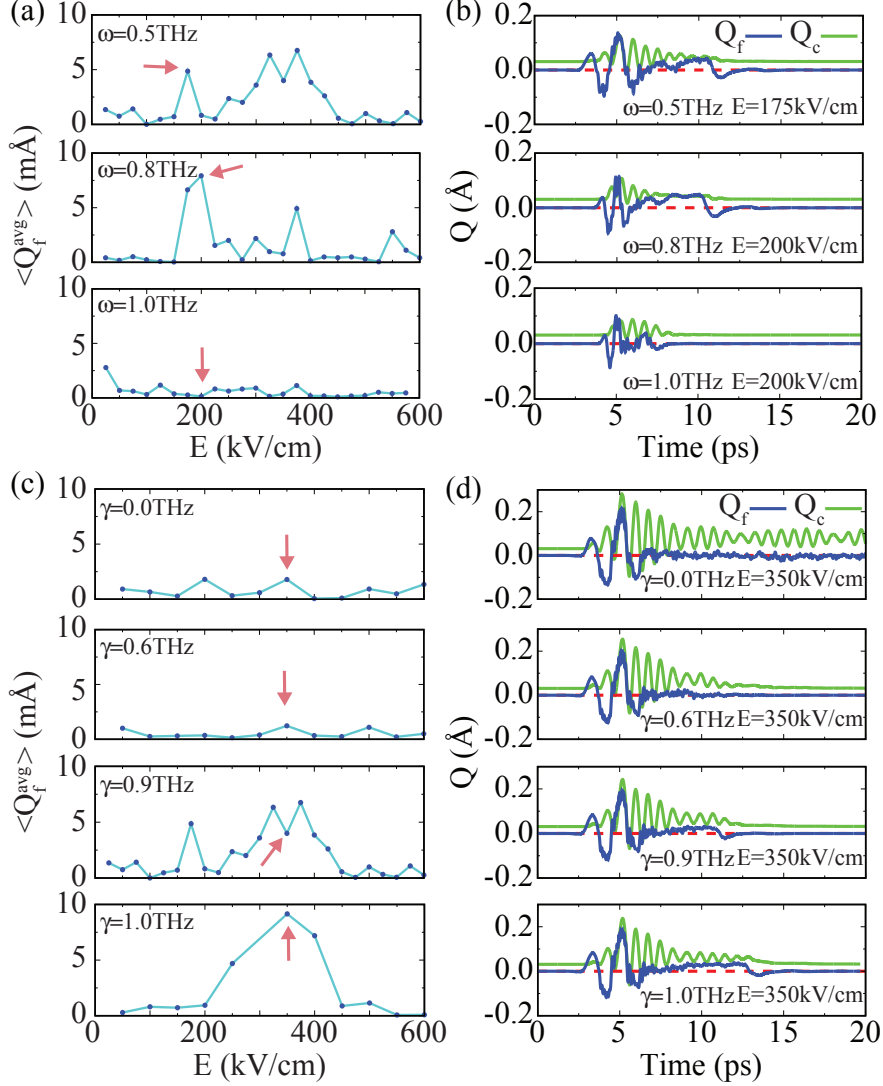


FIG. 3. Effects of frequency and dissipation on THz-induced dynamics in SrTiO₃. (a) Time-averaged value of FES displacement and (b) time profiles of Q_f and Q_c at various THZ frequencies ω and $\gamma = 0.9$ THz. (c) Time-averaged value of the FES displacement and (d) time profiles of Q_f and Q_c at various dissipation rate γ and $\omega = 0.5$ THz. In (a) and (c), the pink arrows indicate the specific points for the time-profiles in (b) and (d).

between ground and first excited states even with near-resonant condition.

We also investigated the effect of the dissipation rate γ on the THz-induced transient ferroelectricity with resonant frequency as shown in Fig. 3(c). Considering that our simplified 2D lattice system does not have other dissipation channels (e.g., electron-phonon and phonon-phonon interactions), the experimentally observed dissipation ratio is required to describe realistic dynamics for this lattice wavefunction. Without dissipation ($\gamma = 0$ THz) and with $\gamma = 0.6$ THz, SrTiO₃ hardly exhibits transient ferroelectricity but provides thermally

excited behavior such as oscillating Q_c (see Fig. 3(d)). On the other hand, the experimentally observed dissipation rate ($\gamma = 0.9$ THz) [33] and higher rates ($\gamma = 1.0$ THz) provide a wide range of field strengths for transient ferroelectricity. These results indicate that realistic dissipation is needed to obtain transient ferroelectricity.

Recently, a plethora of experimental and theoretical studies on light-induced ferroelectricity in perovskite materials have been reported [3, 4, 27, 35, 36]. Among these studies, our results well reproduce the experimental observation of THz field-induced ferroelectricity in SrTiO₃ [3]. In these experiments, a single-cycle THz pulse was applied on SrTiO₃ and resulted in a non-oscillatory SHG signal at optical frequencies, signature of the transient ferroelectric phase. Similar to this observation, we also obtained the non-oscillatory SHG signal and revealed the mechanism underlying this phenomenon. In the same THz-induced SHG traces as well as in optical depolarization signals, the experiments also observed coherent oscillations, indicating the excitation of the anti-ferrodistortive and FES modes in the ferroelectric state. In our simplified lattice model Hamiltonian, the oscillation of the anti-ferrodistortive mode is neglected. Considering the relation between the SHG signal and the FES mode coordinate ($\text{SHG}(Q_f) = \text{SHG}(-Q_f)$), the doubled frequency of the FES in the THz-induced SHG signal indicates paraelectric state which shows the motion of FES mode oscillation over the zero point ($Q_f = 0$). We propose that this behavior of frequency doubling can be experimentally observed under high temperature or high intensity conditions, leading to a thermally excited paraelectric state rather than ferroelectric state.

In conclusion, we investigated THz field-induced transient ferroelectricity in quantum paraelectric SrTiO₃. We solved the time-dependent 2D lattice Schrödinger-Langevin equation to simulate the action of a THz pulse on the material. We found that transient ferroelectricity is realized upon application of a THz pulse with moderate field strength and considering a realistic dissipation rate. The main mechanism of this transient ferroelectricity lies in the excitation between ground and first excited states of the quantum paraelectric phase induced by the symmetry-breaking single-cycle THz pulse. In agreement with previous experimental reports [3, 4], we verified that the non-oscillatory SHG signal is a signature of transient ferroelectricity. We also found that the resonant frequency of the THz pulse and realistic dissipation ratios are required in order to trigger this non-equilibrium phase transition. Our study not only does reproduce the recent experimental observations, but also provides microscopic details that emphasize the importance of the quantum paraelectric

phase in this phenomenon.

We acknowledge financial support from the European Research Council (ERC-2015-AdG-694097), Grupos Consolidados (IT1249-19), JSPS KAKENHI Grant Number 20K14382, the Cluster of Excellence 'CUI: Advanced Imaging of Matter' of the Deutsche Forschungsgemeinschaft (DFG) - EXC 2056 - project ID 390715994. D.S. and S.L. are supported by Alexander von Humboldt Foundation. We also acknowledge support from the Max Planck–New York Center for Non-Equilibrium Quantum Phenomena. The Flatiron Institute is a division of the Simons Foundation.

* dongbin.shin@mpsd.mpg.de

† angel.rubio@mpsd.mpg.de

- [1] M. Mitrano, A. Cantaluppi, D. Nicoletti, S. Kaiser, A. Perucchi, S. Lupi, P. D. Pietro, D. Pontiroli, M. Riccò, A. Subedi, S. R. Clark, D. Jaksch, and A. Cavalleri, *Nature* **530**, 461 (2016).
- [2] T. F. Nova, A. Cartella, A. Cantaluppi, M. Först, D. Bossini, R. V. Mikhaylovskiy, A. V. Kimel, R. Merlin, and A. Cavalleri, *Nat. Phys.* **13**, 132 (2017).
- [3] X. Li, T. Qiu, J. Zhang, E. Baldini, J. Lu, A. M. Rappe, and K. A. Nelson, *Science* **364**, 1079 (2019).
- [4] T. F. Nova, A. S. Disa, M. Fechner, and A. Cavalleri, *Science* **364**, 1075 (2019).
- [5] A. Kogar, A. Zong, P. E. Dolgirev, X. Shen, J. Straquadine, Y.-Q. Bie, X. Wang, T. Rohwer, I.-C. Tung, Y. Yang, R. Li, J. Yang, S. Weathersby, S. Park, M. E. Kozina, E. J. Sie, H. Wen, P. Jarillo-Herrero, I. R. Fisher, X. Wang, and N. Gedik, *Nat. Phys.* **16**, 159 (2020).
- [6] J. Zhang, C. Lian, M. Guan, W. Ma, H. Fu, H. Guo, and S. Meng, *Nano Lett.* **19**, 6027 (2019).
- [7] M. Knap, M. Babadi, G. Refael, I. Martin, and E. Demler, *Phys. Rev. B* **94**, 214504 (2016).
- [8] D. M. Kennes, E. Y. Wilner, D. R. Reichman, and A. J. Millis, *Nat. Phys.* **13**, 479 (2017).
- [9] M.-X. Guan, E. Wang, P.-W. You, J.-T. Sun, and S. Meng, *Nat. Commun.* **12**, 1885 (2021).
- [10] D. Shin, S. A. Sato, H. Hübener, U. D. Giovannini, N. Park, and A. Rubio, *Npj Comput. Mater.* **6**, 182 (2020).
- [11] A. Cantaluppi, M. Buzzi, G. Jotzu, D. Nicoletti, M. Mitrano, D. Pontiroli, M. Riccò, A. Perucchi, P. D. Pietro, and A. Cavalleri, *Nat. Phys.* **14**, 837 (2018).
- [12] M. Budden, T. Gebert, M. Buzzi, G. Jotzu, E. Wang, T. Matsuyama, G. Meier, Y. Laplace,

- D. Pontiroli, M. Riccò, F. Schlawin, D. Jaksch, and A. Cavalleri, *Nat. Phys.* **17**, 611 (2021).
- [13] E. J. Sie, C. M. Nyby, C. D. Pemmaraju, S. J. Park, X. Shen, J. Yang, M. C. Hoffmann, B. K. Ofori-Okai, R. Li, A. H. Reid, S. Weathersby, E. Mannebach, N. Finney, D. Rhodes, D. Chenet, A. Antony, L. Balicas, J. Hone, T. P. Devereaux, T. F. Heinz, X. Wang, and A. M. Lindenberg, *Nature* **565**, 61 (2019).
- [14] C. Vaswani, L.-L. Wang, D. H. Mudiyansele, Q. Li, P. M. Lozano, G. D. Gu, D. Cheng, B. Song, L. Luo, R. H. J. Kim, C. Huang, Z. Liu, M. Mootz, I. E. Perakis, Y. Yao, K. M. Ho, and J. Wang, *Phys. Rev. X* **10**, 021013 (2020).
- [15] J. W. McIver, B. Schulte, F.-U. Stein, T. Matsuyama, G. Jotzu, G. Meier, and A. Cavalleri, *Nat. Phys.* **16**, 38 (2020).
- [16] G. Shirane, K. Suzuki, and A. Takeda, *J. Phys. Soc. Japan* **7**, 12 (1952).
- [17] G. A. Samara, *Ferroelectrics* **2**, 277 (1971).
- [18] L. Bellaiche, A. García, and D. Vanderbilt, *Phys. Rev. Lett.* **84**, 5427 (2000).
- [19] R. Guo, L. E. Cross, S. E. Park, B. Noheda, D. E. Cox, and G. Shirane, *Phys. Rev. Lett.* **84**, 5423 (2000).
- [20] S. Miyasaka, Y. Okimoto, M. Iwama, and Y. Tokura, *Phys. Rev. B* **68**, 100406(R) (2003).
- [21] J. H. Haeni, P. Irvin, W. Chang, R. Uecker, P. Reiche, Y. L. Li, S. Choudhury, W. Tian, M. E. Hawley, B. Craigo, A. K. Tagantsev, X. Q. Pan, S. K. Streiffer, L. Q. Chen, S. W. Kirchoefer, J. Levy, and D. G. Schlom, *Nature* **430**, 758 (2004).
- [22] C. J. Fennie and K. M. Rabe, *Phys. Rev. Lett.* **97**, 267602 (2006).
- [23] J. H. Lee and K. M. Rabe, *Phys. Rev. Lett.* **104**, 207204 (2010).
- [24] K. A. Müller and H. Burkard, *Phys. Rev. B* **19**, 3593 (1979).
- [25] W. Zhong and D. Vanderbilt, *Phys. Rev. Lett.* **74**, 2587 (1995).
- [26] D. Shin, S. Latini, C. Schäfer, S. A. Sato, U. De Giovannini, H. Hübener, and A. Rubio, arXiv preprint arXiv:2101.02291 (2021).
- [27] S. Latini, D. Shin, S. A. Sato, C. Schäfer, U. D. Giovannini, H. Hübener, and A. Rubio, The ferroelectric photo-groundstate of SrTiO_3 : Cavity materials engineering (2021), arXiv:2101.11313 [cond-mat.mtrl-sci].
- [28] See supplemental material at url.
- [29] P. Giannozzi *et al.*, *J. Condens. Matter Phys.* **29**, 465901 (2017).
- [30] J. P. Perdew, K. Burke, and M. Ernzerhof, *Phys. Rev. Lett.* **77**, 3865 (1996).

- [31] S. Garashchuk, V. Dixit, B. Gu, and J. Mazzuca, *J. Chem. Phys.* **138**, 054107 (2013).
- [32] C.-C. Chou, *Ann. Phys.* **362**, 57 (2015).
- [33] M. Kozina, M. Fechner, P. Marsik, T. v. Driel, J. M. Glownia, C. Bernhard, M. Radovic, D. Zhu, S. Bonetti, U. Staub, and M. C. Hoffmann, *Nat. Phys.* **15**, 387 (2019).
- [34] N. Tancogne-Dejean, M. J. T. Oliveira, X. Andrade, H. Appel, C. H. Borca, G. L. Breton, F. Buchholz, A. Castro, S. Corni, A. A. Correa, U. D. Giovannini, A. Delgado, F. G. Eich, J. Flick, G. Gil, A. Gomez, N. Helbig, H. Hübener, R. Jestädt, J. Jornet-Somoza, A. H. Larsen, I. V. Lebedeva, M. Lüders, M. A. L. Marques, S. T. Ohlmann, S. Pipolo, M. Rampp, C. A. Rozzi, D. A. Strubbe, S. A. Sato, C. Schäfer, I. Theophilou, A. Welden, and A. Rubio, *J. Chem. Phys.* **152**, 124119 (2020).
- [35] Y. Ashida, A. İmamoglu, J. Faist, D. Jaksch, A. Cavalleri, and E. Demler, *Phys. Rev. X* **10**, 041027 (2020).
- [36] S. Pal, N. Strkalj, C.-J. Yang, M. C. Weber, M. Trassin, M. Woerner, and M. Fiebig, *Phys. Rev. X* **11**, 021023 (2021).